Journal of Physics: Conference Series

PAPER • OPEN ACCESS

Convective condensation of R449a inside a smooth tube

To cite this article: A Lucchini *et al* 2024 *J. Phys.: Conf. Ser.* **2685** 012062

Convective condensation of R449a inside a smooth tube

A Lucchini[1,*], I M Carraretto[1], L P M Colombo[1], D Mazzeo[1], P G Pittoni[2] and G Lipori[3]

[1] Politecnico di Milano, Via Lambruschini 4, 20156 Milan, Italy
[2] Iowa State University, 2529 Union Drive, Ames, IA 50011, U.S.A.
[3] Lu-Ve S.p.A., via Caduti della Liberazione 53, 21040 Uboldo (VA), Italy

* Corresponding author: andrea.lucchini@polimi.it

Abstract. The HVAC sector has started the phase-out of refrigerants characterized by high values of global warming potential and atmospheric lifetime. Drop-in replacement requires that the new, environmentally safe fluids also show comparable heat transfer performances. This work addresses R449a, a low GWP zeotropic mixture (components: R32, R125, R1234yf, R134a, mass fractions: 24.3%, 24.7%, 25.3%, 25.7%, respectively), suitable to replace both R404A and R507A. Experiments were carried out on condensation in horizontal smooth tubes (outer diameter: 9.52 mm, thickness: 0.3 mm). The range of operating conditions meets the standard for HVAC devices (operating pressure: 14.46 bar, bubble temperature: 30°C, temperature glide: approximately 5 K refrigerant mass flux ranging from 136 to 202 kg m^{-2} s^{-1}, quality change -0.8 and -0.2, mean quality ranging from 0.2 to 0.8). The test section is the inner pipe in a tube-in-tube counter-flow heat exchanger, where the refrigerant is cooled by a demineralized water stream in the annulus. Both the pressure drop and the heat transfer coefficient were measured across a length of 1.3 m and 1.1 m, respectively.

Keywords: *Convective condensation, R449a, heat transfer coefficient, pressure drop, smooth tube*

1. Introduction

Refrigerants are widely used in many industrial and domestic applications, such as refrigeration, air conditioning and power generation. Since the 1987 Montreal Protocol, the environmental issue has been one of the most important, leading to the development of new refrigerants. The HVAC sector is undergoing the replacement of hydrofluorocarbons (HFCs) with lower GWP, environmentally friendly refrigerants. The hydrofluoroolefins (HFOs) and the mixtures of hydrofluorocarbons and hydrofluoroolefins (HFC+HFO) are among the candidates. The mixtures allow for the mitigation of the flammability concerns of some pure HFOs, meeting the constraints on the GWP, and keeping similar performances to their HFC predecessors. On the other hand, many mixtures show zeotropic behavior. That makes the description of the phase change more complex compared to pure fluids. Condensation starts at the dew point temperature and ends at the bubble point temperature. Furthermore, coupling between heat and mass transfer takes place. Close to the vapour-liquid interface, concentration gradients develop in the vapor phase due to the preferential condensation of the less volatile component. The

Table 1. R449A composition.

Component		R32	R125	R1234yf	R134a
Atmospheric lifetime	[days]	1790	10600	11	5100
Mass fraction	[$kg_i \cdot kg_{tot}^{-1}$]	24.3%	24.7%	25.3%	25.7%
Molar mass	[$kg \cdot kmol^{-1}$]	86.5	120.0	114.0	102.0
GWP	[-]	675	3500	4	1430

Table 2. R449A properties.

Critical pressure	[bar]	44.47
Critical temperature	[°C]	81.5
Temperature glide	[°C]	4.47
Molar mass	[$kg \cdot kmol^{-1}$]	87.2
GWP.	[-]	1397

Table 3. Smooth tube geometrical features

Inner diameter	[mm]	D_I	8.92
Outer Diameter	[mm]	D_O	9.52
Wet perimeter	[mm]	P	28.0
Cross section area	[mm^2]	A	62.5
Hydraulic diameter	[mm]	D_H	8.92

Table 4. Uncertainties affecting the heat transfer coefficient

Mass flow rate (water/refrigerant)	[-]	± 0.15% of the reading
Temperature	[K]	± 0.1
Operating pressure	[bar]	± 0.025
Pressure drop	[kPa]	± 0.037
Evaporator power	[kW]	± 0.09

increased concentration of the more volatile components reduces the interface temperature, resulting in a lower driving temperature difference and degrading the heat transfer.

To properly design HVAC devices, a lot of efforts have been made to test the heat transfer features of the new refrigerants and to develop suitable correlations to predict the pressure gradient and the heat transfer coefficient during boiling and condensation. Muller-Steinhagen and Heck [1] and Nozu et al. [2] developed correlations to predict the former quantity for smooth tubes. Cavallini et al. [3] [4] [5] proposed a method to predict both the quantities for pure fluids flowing into horizontal smooth or micro-fin tubes. Similarly, Kedzierski and Goncalves [6], working on four different refrigerants (R134a, the near-azeotropic refrigerant mixture R410A and its pure components R125 and R32), provided a model to compute both the quantities during convective condensation inside micro-fins tube. On the other hand, Kumar et al. [7] experimentally evaluated heat transfer during condensation of pure R134a inside a micro-fin tube for different tube inclinations and developed a new correlation. The authors found that, as the condensation proceeds, for all the possible inclination angles a decrease in the heat transfer coefficient is depicted: this is explainable by looking at the augmentation in the average thickness of condensate film which offers higher thermal resistance to the heat flux. A further correlation to compute the heat transfer coefficient was developed by Deng et al. [8].

As many correlations were developed working on pure fluids, they are unable to account for the mass transfer resistance at the liquid-vapor interface and the corresponding reduction in heat transfer. To extend their feasibility to zeotropic mixture Bell and Ghaly [9] proposed a correction.

2. Experimental setup

The tests focused on R449a (a zeotropic mixture made of 4 pure refrigerants, composition in Table 1, properties in Table 2), which is one of the possible drop-in replacements for the refrigerants R404A (GWP 3922) and R507A (GWP 3985). A concise description of the experimental setup (Figure 1), made up of three circuits, follows (an extended version is available in Colombo et al. [10]).

In the refrigerant loop (red line in Figure 1), a shell-and-tube condenser feeds the pump with liquid refrigerant. To prevent cavitation, after the condenser, a plate heat exchanger (sub-cooler) chills the liquid refrigerant. The mass flow rate is fixed by a gear pump with an inverter drive while its value is measured by a Coriolis flow meter (range: 0÷400 $kg \cdot h^{-1}$, uncertainty: ±0.15% of the reading). The thermodynamic state of the refrigerant is monitored by a thermocouple (K type, uncertainty: ±0.1 K) and a pressure transducer (range: -1÷30 bar, uncertainty: ±1% of full scale) as it enters the electric evaporator (power 9 kW). A software tunes its thermal power to get a two-phase flow in suitable conditions. To reach thermal equilibrium between liquid and vapor, a coiled tube (length: 12m, coil diameter: 0.7m, coil axis perpendicular to gravity) is installed at the evaporator outlet. Then, for the development of the flow regime, a straight adiabatic calming section (length: 4.7 m. inner diameter 8.92 mm) is adopted. Subsequently, the refrigerant enters the test section, (tube-in-tube counter flow heat exchanger, distance between the pressure taps: L=1.3 m, heat transfer length: l=1.11 m, thermal insulation: rubber foam, thickness: 100 mm). The refrigerant flows in the inner tube (geometrical features in Table 3) while demineralized water flows in the annulus. The refrigerant inlet pressure is measured by an absolute pressure transducer (range: 0÷16 bar, uncertainty: ±0.25% of full scale) while

the pressure drop is read by a differential pressure transducer (range: -1.0÷1.0 bar, uncertainty ±0.1% of full scale). The refrigerant inlet and outlet temperatures are provided by two thermocouples (K type, uncertainty: ±0.1 K) while the wall temperature is computed as the average value of three thermocouples glued in grooves (length: 50mm, depth: 0.15mm, width: 0.4mm) machined on the outside of the inner tube (top, side, bottom positions). A group is at the inlet and another is at the outlet. The reference junctions of all the thermocouples installed in the test section are placed in Dewar flasks filled with melting ice. Then the refrigerant returns to the condenser.

The water circuit (green line in Figure 1) exchanges thermal power with the refrigerant in the test section to induce phase change. The water mass flow rate is measured by a Coriolis flowmeter (range: 0÷400 kg·h^{-1}, uncertainty of ±0.15% of reading). A thermally insulated tank supplies the water flow, which is controlled using a bypass or needle valve. Subsequently, the water is cooled in a plate heat exchanger (glycol flushed on the other side for cooling) then a PID-driven electric heater (6 kW), sets the inlet temperature in the test section, which is measured, like the outlet temperature, using a group of 3 thermocouples connected in series (K type, uncertainty: ±0.1 K). The power supply causes a prescribed temperature change in the water flow.

In the glycol loop (blue line in Figure 1), a tank stores a mixture of water and glycol (30% volume concentration, freezing temperature -17°C, temperature -10°C) produced by a commercial chiller (cooling capacity of 21 kW). Two separate circuits, one for water and the other for the refrigerant, supply the heat exchangers. The former loop cools the demineralized water. The latter controls the refrigerant pressure at the test section inlet and prevents cavitation in the refrigerant pump. To achieve the former goal, a manual needle valve sets the mass flow rate and a PID-driven electric heater (3 kW) tunes the condenser inlet temperature to match the refrigerant saturation pressure at the test section inlet. A bypass drains the glycol to cool the liquid refrigerant leaving the condenser.

3. Data sampling

During a test, 181 samples were collected for each quantity (sampling frequency: 1 Hz) and their mean values are the output. The acquisition procedure, to check the repeatability, prescribes, for each experiment, to repeat 10 tests, and their mean values are the output. The operating conditions are univocally defined by four parameters:

1. the refrigerant pressure at the test section inlet (p_{rTi});
2. the refrigerant mass flux (G);
3. the quality variation in the test section (Δx);
4. the mean quality in the test section (x_m).

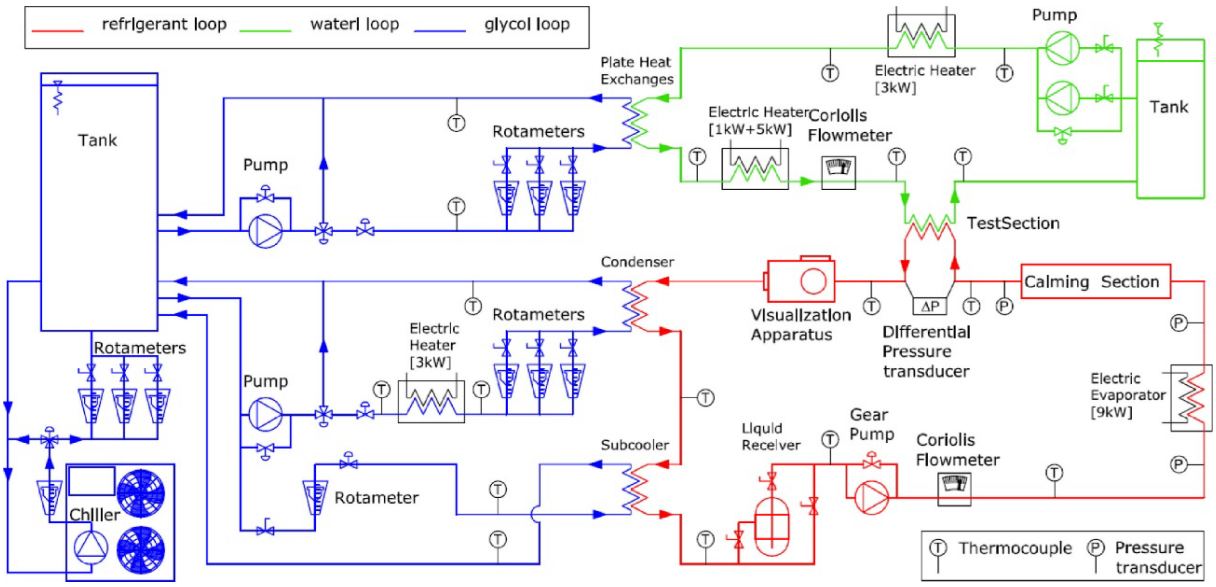

Figure 1. Scheme of the experimental setup and three circuit loops.

4. Data processing

Once an experiment is completed the readings of the instruments are processed assuming:

- steady-state operating conditions (the data are processed only if the oscillations of the quantities are smaller than ±3% and the temperatures oscillate within ±0.2 K);
- negligible thermal dispersions (single phase tests proved that, in the test section, the refrigerant side thermal power and the waterside thermal power differ at most of 5%);
- negligible thermal resistance of the copper tube (a posteriori calculation shows that it is two orders of magnitude smaller than the refrigerant thermal resistance);
- negligible fouling effect (the refrigerant circulation pump is gear-type magnetically driven and does not require lubricant).

The post-processing provides three outputs: the operating conditions (p_{rTi}, G, Δx, x_m), the total pressure drop per unit length (Z) and the heat transfer coefficient (h). Their uncertainties are evaluated with the uncertainty propagation algorithm described by Moffat [11]. For a quantity y which depends on n independent variables x_j, the absolute uncertainty U_y is:

$$U_y = \sqrt{\sum_{j=1}^{n} \left(U_{x_j} \frac{\partial y}{\partial x_j} \right)^2} \tag{1}$$

The refrigerant pressure at the test section inlet p_{rti} is the reading of the absolute pressure transducer while the temperature at the same location T_{rti} is provided by a thermocouple.

Mass flux G is the ratio of the refrigerant mass flow rate m_r and the duct cross-sectional area (A_c):

$$G = \frac{m_r}{A_c} \tag{2}$$

The refrigerant quality change in the test section is computed from the refrigerant conditions, defined by pressure and enthalpy, at the inlet and outlet sections.

- The outlet pressure p_{rto} is determined by subtracting the pressure drop ($\Delta p>0$) measured by the differential pressure transducer from the inlet pressure:
$$p_{rTo} = p_{rTi} - \Delta p \tag{3}$$
- The test section inlet enthalpy i_{rti} is computed by the energy balance at the evaporator. The enthalpy of the subcooled liquid at the evaporator inlet i_{rei} is the output of NIST software RefProp 10 on the base of the temperature T_{rei} and pressure p_{rei} at the evaporator inlet:
$$i_{rEi} = i(T_{rEi}, p_{rEi}) \tag{4}$$
The thermal power Q_E, provided by the evaporator, is measured by a net-analyzer and the evaporator outlet enthalpy, which matches with the enthalpy at the test section inlet, is:
$$i_{rTi} = i_{rEi} + \frac{Q_E}{m_r} \tag{5}$$
- The test section outlet enthalpy i_{rto} is determined by the energy balance at the test section:
$$i_{rTo} = i_{rTi} + \frac{m_a c_{pa} (T_{aTi} - T_{aTo})}{m_r} \tag{6}$$

The inlet quality x_{Ti} and the outlet quality x_{To} are computed employing RefProp 10 providing, as inputs, the pressure and the enthalpy at the corresponding position:

$$x_{Ti} = x(p_{rTi}, i_{rTi}) \tag{7}$$
$$x_{To} = x(p_{rTo}, i_{rTo}) \tag{8}$$

The difference between the last two quantities is the quality change Δx, while their average is the mean quality x_m

$$\Delta x = x_{Ti} - x_{To} \tag{9}$$
$$x_m = \frac{x_{To} + x_{Ti}}{2} \tag{10}$$

A differential pressure transducer provides the total pressure drop Δp (accelerative component and frictional component) on the test section while the distance between the pressure taps (L=1.3 m) was measured when the test section was built. The pressure gradient Z (uncertainty smaller than 4%) is:

$$Z = \frac{\Delta p}{L} \tag{11}$$

The heat transfer coefficient h, referred to the tube's inner surface, is computed using the logarithmic mean temperature difference ΔT_{ml}, which calculation relays on the refrigerant and wall temperatures. The wall temperatures are computed as the averages of the readings of the thermocouple glued on the outside of the copper tube separating the refrigerant and the water:

$$T_w = \frac{T_b + T_s + T_t}{3} \tag{12}$$

Accordingly, the logarithmic mean temperature difference is:

$$\Delta T_{lm} = \frac{(T_{wo} - T_{rTo}) - (T_{wi} - T_{rTi})}{\ln \frac{T_{wo} - T_{rTo}}{T_{wi} - T_{rTi}}} \tag{13}$$

Such quantity allows computing the refrigerant heat transfer coefficient:

$$h = \frac{Q_T}{\pi D_I l \Delta T_{lm}} \tag{14}$$

As the thermocouple providing T_{rTo} is close to the test section outlet, the distance between them might be too short to guarantee thermal equilibrium between liquid and vapor, which could make the reading not reliable. A viable option, to overcome that issue, is represented by computing the temperature difference between the inlet and outlet, assuming thermodynamic equilibrium between the phases at both locations:

$$t_{rT} = T(p_{rTo}, i_{rTo}) - T(p_{rTi}, i_{rTi}) \tag{15}$$

Then, such difference is added to the refrigerant inlet temperature:

$$T_{rToc} = T_{rTi} + t_{rT} \tag{16}$$

The corrected refrigerant outlet temperature T_{rToc} replaces the measured refrigerant outlet temperature T_{rTo} in equation (14) to compute the corrected logarithmic mean temperature difference ΔT_{lmc} and then, the corrected heat transfer coefficient h_c using equation (15). Accordingly to the data reported in Table 4, the uncertainty related to the heat transfer coefficient, regardless of the procedure adopted, is not larger than 8%.

5. Results

The tests can be grouped into two categories: complete condensation and partial condensation, both performed by setting the test section inlet pressure at pressure p_{rTi}=14.46 bar (bubble temperature 30°C).

- Complete condensation aims to simulate real operating conditions, different mass fluxes were tested, while the quality change and the mean quality were fixed (G∈[136;202] kg·m^{-2}·s^{-1}, q∈[27.6;70.2] kW m^{-2}, Δx=-0.8, x_m=0.5, red circles in Figure 2).
- Partial condensation aims to highlight the effect of the mean quality, while the mass flux and the quality change were fixed (G = 202 kg·m^{-2}·s^{-1}, q=17.5 kW m^{-2}, Δx=-0.2, x_m∈[0.2;0.8], blue circles in Figure 2).

As reported in the open literature [12] on a technical point of view, with respect to heat transfer, the best operating conditions are for mass fluxes larger than 150 kg·m^{-2}·s^{-1}, for which a consistent portion of the perimeter is wetted by the liquid (almost uniform liquid thickness).

During complete condensation (Figure 3), the total pressure gradient Z versus the mass flux G is a nearly quadratic function (power law fitting provides: n=2.19, cn=4.32·10-3 s-1).

Figure 4 shows, for complete condensation tests, the heat transfer coefficients h and h_c and their percentage difference Δh% versus the mass flux G, while Figure 5 displays, for the partial condensation tests, the same quantities versus the mean quality x_m. In both cases, the percentage difference between

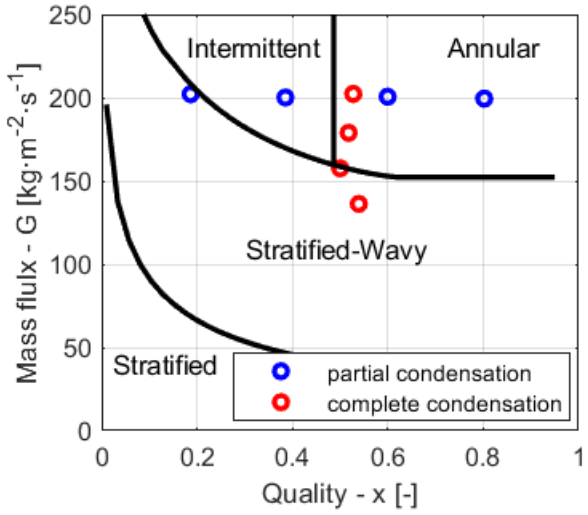

Figure 2. Operating conditions tested reported on the Kattan flow pattern map [13].

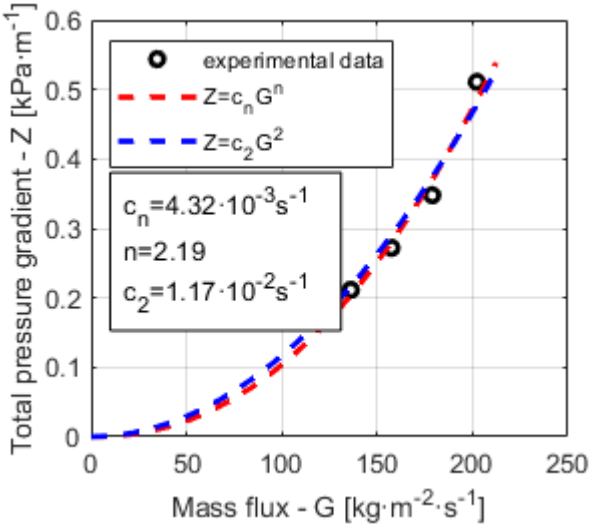

Figure 3. Total pressure gradient Z vs mass flux G during complete condensation (x_m=0.5, Δx=0.8).

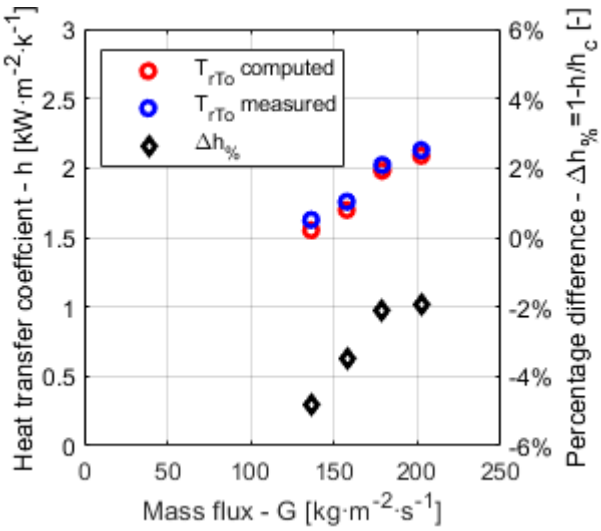

Figure 4. Heat transfer coefficient during h vs mass flux G during complete condensation (x_m=0.5, Δx=0.8).

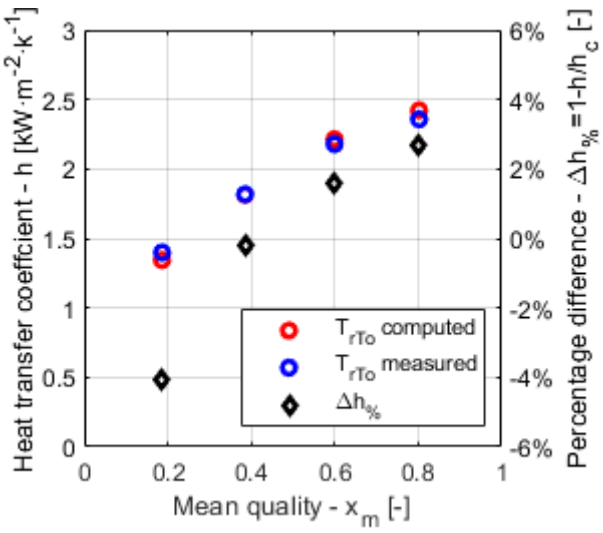

Figure 5. Heat transfer coefficient h vs mean quality x_m during partial condensation (G=202 kg·m^{-2}·s^{-1}, Δx=0.2).

the heat transfer coefficients is always within ±5%, which means that it is acceptable to assume thermal equilibrium at the test section outlet.

To analyze the heat transfer performances it is useful to highlight some remarks.

A. The density of the liquid phase (ρ_l=1070kg·m^{-3}) is almost twenty times larger than the density of the vapor phase (ρ_v=58.9kg·m^{-3}).
B. The thermal conductivity of the liquid phase (k_l=7.72·10^{-2}W·m^{-1}·K^{-1}) is almost five times larger than the thermal conductivity of the vapor phase (k_v=1.55·10^{-2}W·m^{-1}·K^{-1}).
C. Because of remark A, during the experiments, the vapor occupied the largest part of the cross-sectional area (e.g. case x=0.1, the volume quality is 67%).
D. In the stratified-wavy flow, the liquid lies in the lower part of the tube because the gravity effect overcomes the shear stress effect. The heat transfer performances of the flow are mainly related to the vapor thermal conductivity.
E. In the intermittent flow the effects of gravity and shear stress are comparable and, periodically, the liquid is capable of adjoining a significant portion of the cross-sectional

Table 5. parameters used to benchmark the prediction capability of the correlations

Meaning	equation	n°	meaning	equation	n°
Percentage error of the j-th operating conditions	$E_{j\%} = \frac{g_{Cj} - g_{ej}}{g_{ej}}$	(17)	Mean absolute percentage error	$E_{A\%} = \sum_{j=1}^{n} \frac{\lvert E_{j\%} \rvert}{n}$	(19)
Mean percentage deviation	$E_{\%} = \sum_{j=1}^{n} \frac{E_{j\%}}{n}$	(18)	Standard deviation of the mean percentage error	$s = \sqrt{\sum_{j=1}^{n} \frac{\left(E_{j\%} - E_{\%}\right)^2}{n}}$	(20)

Table 6. Pressure drop: correlations performances

Correlation	$E_{\%}$	$E_{A\%}$	$s_{\%}$
Cavallini et al.	-3.0%	19.0%	21.3%
Kedzierski and Goncalves	-32.4%	32.6%	25.5%
Muller-Steinhagen and Heck	-23.6%	23.6%	16.7%
Nozu et al.	11.7%	33.7%	39.9%

Table 7. Heat transfer coefficient: correlations performances

Correlation	$E_{\%}$	$E_{A\%}$	$s_{\%}$
Cavallini et al.	13.9%	13.9%	7.5%
Deng et al.	10.5%	10.5%	4.3%
Kedzierski and Goncalves	-6.9%	7.9%	7.6%
Kumar et al.	-6.2%	7.5%	6.6%

perimeter. The heat transfer performances of the flow are influenced by the thermal conductivities of both liquid and vapor.

F. In the annular flow the shear stress effect overcomes the gravity effect and the liquid arranges, in an almost uniform layer, all around the cross-sectional perimeter. The heat transfer performances of the flow are mainly related to the liquid thermal conductivity.

G. As long as the quality change Δx and the mean quality x_m are the same, because of remarks B, E and F, it could be expected that the heat transfer performance of intermittent flow is better than the stratified-wavy flow and worse than the annular flow.

Complete condensation tests (Figure 4) highlight a slope change of the heat transfer coefficient trend in the range G=[150; 200] kg·m^{-2}·s^{-1}. That could be related, as the mass flux increases (Figure 3), to the transition from the stratified-wavy flow to the intermittent flow and annular flow because of remark G. The experiment concerning partial condensation (Figure 5) further supports the explanation. As the mean quality increases the flow regime shifts from stratified-wavy to intermittent flow and, in the end, to annular flow. In agreement with remark G, the heat transfer coefficient grows. The slope reduction shifting from x_m=0.6 to x_m=0.8 could be explained because annular flow onset in both operating conditions and the heat transfer coefficient increase is related only to the larger vapor velocity and thinner liquid annulus, as mentioned by Kumar et al. [7].

The correlations' capability to predict the experimental data is quantified using the parameters reported in Table 5. The results concerning the total pressure gradient Z are summarized in Table 6. Only two of the four selected correlations can provide predictions of the experimental data within ±30%, the best performing is the Cavallini et al. [5] correlation (mean absolute percentage error +19%) even though the Muller-Steinhagen and Heck [1] provides similar absolute deviation but shows a tendency towards underestimation. On the contrary, as shown in Table 7, all the selected correlations, with the Bell and Ghaly [9] correction, provide good performances, the absolute percentage error, for all of them, is smaller than 15% and for the Kumar et al. [7] correlation, which is the best performing (mean absolute percentage error 7.5%).

6. Conclusions

The manuscript reports the investigation of the heat transfer performance (total pressure gradient and heat transfer coefficient) of the refrigerant R449A during convective condensation inside a horizontal smooth tube. Complete condensation showed that a nearly quadratic power-law interpolation curve fits well with the total pressure gradient as a function of the mass flux. Moreover, both the complete and partial condensation experiments highlight the effect of the flow regime transition on the heat transfer coefficient. The correlation benchmark pointed out that the predictions of the pressure gradient showed a limited agreement with the data, the Cavallini et al [5] correlation, which is the best performing, has a 19% mean absolute percentage error. On the contrary, the correlations for the heat transfer coefficient, with the Bell and Ghaly [9] correction, prove a good predictive capability, mean absolute percentage error lower than 15%.

7. Nomenclature

Latin symbols

symbol	meaning	units	symbol	meaning	units
A	cross sectional area	[m^2]	n	number of elements	[-]
c_p	specific heat capacity	[$J \cdot kg^{-1} \cdot K^{-1}$]	p	refrigerant pressure	[Pa]
D	diameter	[m]	P	wet perimeter	[m]
$E_{\%}$	mean percentage error	[-]	Q	thermal power exchanged	[W]
G	refrigerant mass flux	[$kg \cdot m^{-2} \cdot s^{-1}$]	s	standard deviation	[-]
g	generic quantity	[-]	T	temperature	[K]
h	heat transfer coefficient	[$W \cdot m^{-2} \cdot K^{-1}$]	t	temperature difference	[-]
i	specific enthalpy	[$J \cdot kg^{-1}$]	U	absolute uncertainty	[-]
L	pressure taps distance	[m]	x	refrigerant quality	[-]
l	heat transfer length	[m]	y	independent variable	[-]
m	mass flow rate	[$kg \cdot s^{-1}$]	z	pressure gradient	[$Pa \cdot m^{-1}$]

Greek symbols

symbol	meaning	units	symbol	meaning	units
Δp	pressure drop	[Pa]	Δx	test section quality change	[-]

Subscripts

symbol	meaning	symbol	meaning
a	water	j	j-th element
A	absolute	lm	log mean
b	bottom	m	mean
C	correlation	o	outlet
c	corrected	O	outer
E	evaporator	r	refrigerant
e	experimental	s	side
H	hydraulic	t	top
i	inlet	T	test section
I	inner	w	wall

8. References

[1] H. Muller-Steinhagen and K. Heck. A simple friction pressure drop correlation for two-phase flow in pipes. Chemical Engineering and Processing, 20:297–308, 1986.
[2] H. Nakata S. Nozu, H. Katayama and H. Honda. Condensation of a refrigerant cfc11 in horizontal microfin tubes (proposal of a correlation equation for frictional pressure gradient). Experimental Thermal and Fluid Science, 18:82–96, 1998.
[3] L. Doretti G.A. Longo A. Cavallini, D. Del Col and L. Rossetto. Pressure drop during condensation and vaporisation of refrigerants inside enanched tubes. Heat and Technology, 15(1):3–10, 1997.
[4] L. Doretti M. Matkovic L. Rossetto C. Zilio G. Censi A. Cavallini, D. Del Col. Condensation in horizontal smooth tubes: a new heat transfer model for heat exchanger design. Heat Transfer Eng., 27:31–38, 2006.
[5] S. Mancin L. Rossetto A. Cavallini, D. Del Col. Condensation of pure and near- azeotropic refrigerants in microfin tubes: A new computational procedure. International Journal of Refrigeration, 32:162–174, 2009.
[6] M.A. Kedzierski and J.M. Goncalves. Horizontal convective condensation of alternative refrigerants within a micro-fin tube. Journal of Enhanced Heat Transfer, 6:161–178, 1999.
[7] R. Kumar M.A. Akhavan-Behabadi and S.G. Mohseni. Condensation heat transfer of r- 134a inside a microfin tube with different tube inclinations. International Journal of Heat and Mass Transfer, 50:4864– 4871, 2007.
[8] M. Fernandino H. Deng, M. Rossato and D. Del Col. A new simplified model for condensation heat transfer of zeotropic mixtures inside horizontal tubes. Applied Thermal Engineering, 153:779–790, 2019.
[9] M. Ghaly K. Bell. An approximate generalized design method for multicomponent/partial condensers. AIChE symposium series, 69:72–79, 1973.
[10] L. P. M. Colombo, A. Lucchini, T. Nhan Phan, L. Molinaroli, and A. Niro, "Design and assessment of an experimental facility for the characterization of flow boiling of azeotropic refrigerants in horizontal tubes," J. Phys. Conf. Ser., vol. 1224, no. 1, 2019
[11] Moffat, R.J., "Describing the uncertainties in experimental results,"Exp.Therm. and Fluid Sci.,1(1), pp 3-17, (1988).
[12] Hewitt, G. F. and Barbosa, J., "Heat exchanger design handbook", 98. Begell house New York, 2008.
[13] Kattan, N., Thome, J.R., Favrat, D.,"Flow boiling in horizontal tubes: part 1-development of a diabatic two-phase flow pattern map,"J. Heat Transfer, 120(1), pp. 140–147, (1998).

Acknowledgements

This study was carried out within the NEST - Network 4 Energy Sustainable Transition (D.D. 1243 02/08/2022, PE00000021) and received funding under the National Recovery and Resilience Plan (NRRP), Mission 4 Component 2 Investment 1.3, funded from the European Union - NextGenerationEU. This manuscript reflects only the authors' views and opinions, neither the European Union nor the European Commission can be considered responsible for them.